

Photoelectron Imaging of Hydrated Carbon Dioxide Cluster Anions

Eric Surber, Richard Mabbs, Terefe Habteyes, and Andrei Sanov*

Department of Chemistry, University of Arizona, Tucson, Arizona 85721-0041

Received: January 5, 2005; In Final Form: March 3, 2005

The effects of homogeneous and heterogeneous solvation on the electronic structure and photodetachment dynamics of hydrated carbon dioxide cluster anions are investigated using negative-ion photoelectron imaging spectroscopy. The experiments are conducted on mass-selected $[(\text{CO}_2)_n(\text{H}_2\text{O})_m]^-$ cluster anions with n and m ranging up to 12 and 6, respectively, for selected clusters. Homogeneous solvation in $(\text{CO}_2)_n^-$ has minimal effect on the photoelectron angular distributions, despite dimer-to-monomer anion core switching. Heterogeneous hydration, on the other hand, is found to have the marked effect of decreasing the photodetachment anisotropy. For example, in the $[\text{CO}_2(\text{H}_2\text{O})_m]^-$ cluster anion series, the photoelectron anisotropy parameter falls to essentially zero with as few as 5–6 water molecules. The analysis of the data, supported by theoretical modeling, reveals that in the ground electronic state of the hydrated clusters the excess electron is localized on CO_2 , corresponding to a $(\text{CO}_2)_n^-(\text{H}_2\text{O})_m$ configuration for all cluster anions studied. The diminishing anisotropy in the photoelectron images of hydrated cluster anions is proposed to be attributable to photoinduced charge transfer to solvent, creating transient $(\text{CO}_2)_n^-(\text{H}_2\text{O})_m^-$ states that subsequently decay via autodetachment.

1. Introduction

Fascinating in their own right, gas-phase clusters are often thought of as model systems for examining the molecular-level interactions implicated in solvation and the chemistry of condensed environments.^{1–3} Especially notable in this regard are clusters carrying an excess electron. In the realm of cluster anions, experiments focus on the structure of the core anion and the solvation shell, as well as the solvent-induced dynamics: recombination, charge transfer to solvent, and other solvent mediated processes.^{3,4}

The present work pursues a study of the equilibrium charge localization and photoinduced electron detachment in mixed, negatively charged clusters of water and carbon dioxide. The effect of hydration on the electronic structure of ions has far-reaching implications for the chemistry of the atmosphere, seawater, aerosols, and other biologically and environmentally important systems. The ionic interactions are particularly important when the corresponding neutral molecule itself does not bind an excess electron, yet the solvent-induced interactions facilitate electron capture, stabilizing the anion within a cluster. Besides the energetic effect, solvation can dramatically affect the electronic structure and even lead to the formation of new chemical bonds. Remarkable examples of such behavior are the $(\text{CO}_2)_n^-$, $(\text{OCS})_n^-$, and $(\text{CS}_2)_n^-$ cluster anions.^{5–11} In each of these cluster families, new chemical bonds are formed in the clusters of selected sizes in the presence of an excess electron, yielding covalently bound dimer-anion cores.^{10–13}

The above are examples of homogeneously solvated cluster anions, X_n^- , in which the solvent is composed of the same type of molecules as the core anion itself. The term “homogeneous” in this context does not imply that the excess charge is distributed uniformly throughout the cluster. On the contrary, in many cases the excess electron is predominantly localized on a well-defined core moiety. The properties of the core are fundamental to the cluster reactivity and dynamics and the central question in this regard is what causes the electron to

localize on a single molecular group or be shared between two (or more) moieties.

In mixed cluster anions, described as $(X_nY_m)^-$, different identities of X and Y, particularly the differing electron affinities, often cause the excess electron to gravitate toward one of the constituents. The resulting cluster can be described as either $X_n^- \cdot Y_m$ or $X_n \cdot Y_m^-$. Well-studied examples of such systems are $\text{I}_2^- \cdot \text{Ar}_n$, $\text{I}_2^- (\text{CO}_2)_n$, $\text{I}^- (\text{H}_2\text{O})_n$ and similar cluster anions, where the relatively large electron affinity of molecular or atomic iodine is responsible for the charge localization. Even so, the diffuse electronic wave functions of negative ions allow for substantial overlap with the surrounding solvent. For example, even in such a relatively small cluster anion as $\text{I}^- \cdot \text{CO}_2$, Neumark and co-workers observed a 175 °CO₂ bond angle, attributed either to a small amount of charge transfer from the I^- and/or due to electrostatic interaction between the partial charges in the complex.^{14–18} The experiments by Johnson and co-workers on hydrated cluster anions indicate the profound effect that the charge density has on the structure adopted by a water network bound to an ion.^{19–25} Charge delocalization is intuitively expected to become more important in larger solvated systems, where in addition to the delocalization in the ground state, charge-transfer-to-solvent excited states may become available, as observed in both the bulk environments^{26,27} and gas-phase clusters.^{4,28–34}

The hydrated carbon dioxide cluster anions considered in the present work are different from the above examples in that neither CO_2 nor H_2O possess positive electron affinities in isolation, yet both bind electrons in the respective homogeneous cluster forms. These properties set the stage for an intriguing interplay between the CO_2 and H_2O segments of the mixed $[(\text{CO}_2)_n(\text{H}_2\text{O})_m]^-$ cluster anions.

Pure water cluster anions have long served as favorite systems for the studies of electron solvation and reactivity and the transition between the gas-phase and bulk properties.^{35–39} The variety of interactions in these clusters, including hydrogen bonding and delocalized-charge-dipole interactions, lead to

significant molecular rearrangements and interesting structure variations upon electron attachment.^{38,40–42} Spectroscopy of (CO₂)_n[−],^{5,7,43,44} on the other hand, has also revealed evidence for different core-anion structures.^{12,44,45} The (CO₂)_n[−], $n = 2–5$, clusters are composed of a covalently bound dimer anion core solvated by the remaining $n - 2$ neutral molecules, whereas for $n > 6$ the cluster core “switches” to a monomer anion.⁵

Heterogeneous cluster anions have not been studied as extensively. One relevant example is the hydration of OCS[−],^{46,47} which is characterized by a nonexistent (slightly negative) adiabatic electron affinity of neutral carbonyl sulfide.^{46–48} In this light, the case of mixed CO₂ and H₂O cluster anions is more intriguing, because the adiabatic electron affinity of CO₂ is markedly negative (−0.6 eV).^{49,50} The effect of hydration by just one water molecule was studied in (CO₂)_n[−]·H₂O cluster anions following their first observation by Klots.⁵¹ A picture reminiscent of the pure (CO₂)_n[−] clusters has emerged from the measurements and theoretical calculations by Nagata and co-workers, who observed the coexistence of monomer and dimer anion cores in (CO₂)_n[−]·H₂O for $n = 2–4$, followed by an apparent switch to just one core type, CO₂[−], for $n > 4$.^{6,8,9,52}

The adaptation^{17,47,53–55} of the imaging approach^{56,57} to negative-ion photoelectron spectroscopy⁵⁸ opened a new chapter in the studies of cluster-anion structure and dynamics. Photoelectron images reveal the energetics of the detachment process, as well as the photoelectron angular distributions (PAD), unraveling signatures of the molecular orbitals from which the detachment takes place.⁵⁴ Recently, our group used photoelectron imaging to examine the effects of solvation and core-switching on the photoelectron angular distributions in (CO₂)_n[−] and (CO₂)_n[−]·H₂O.⁵⁹ We found that the different anionic cluster cores exhibit very similar PADs, skewed along the laser polarization. The analysis rationalized this observation as resulting from the common origin of the monomer and dimer-anion orbitals.⁶⁰

The focus of the present work is on the structure and detachment dynamics of mixed CO₂–water cluster anions in the presence of more than one water molecule. Given the ability of water molecules to (collectively) bind an excess electron, qualitatively different structural effects can be expected, a priori, in cluster anions hydrated by several H₂O groups, compared to (CO₂)_n[−] and (CO₂)_n[−]·H₂O. In relatively large mixed clusters, one might expect competition between the CO₂ and H₂O segments for binding the excess charge. In addition, the possibility of photoinduced electron transfer between the two cluster constituents must be considered.

2. Experimental Apparatus

The experimental apparatus has been described in detail elsewhere.^{46,54} In brief, it employs the ion generation and mass analysis techniques introduced by Lineberger and co-workers,^{61,62} combined with a velocity mapped,⁶³ imaging⁵⁶ scheme for detection of the photoelectrons.

The [(CO₂)_n(H₂O)_m][−] cluster anions are formed by expansion of undried CO₂ at a stagnation pressure of 0–20 psig through a pulsed (70 Hz) nozzle (General Valve Series 9) into a vacuum chamber with a base pressure of 10^{−6} Torr, rising to 2 × 10^{−5} Torr when the valve is operated. A residual water trace within the delivery lines serves as a source of H₂O. The supersonic expansion is crossed with a 1 keV electron beam and the anions are pulse extracted into a Wiley–McLaren time-of-flight mass spectrometer.⁶⁴ After passing through the acceleration stack, several sets of ion optics^{46,54} and a fast potential switch,⁶⁵ the ions enter the detection region with a typical base pressure of

3 × 10^{−9} Torr. Mass selection is ensured by ion time-of-flight detection using a dual microchannel plate (MCP) detector (Burle, Inc.) at the end of the apparatus.

Before impacting the ion detector, the ion beam is crossed with the frequency doubled output beam from an amplified Ti:Sapphire laser system (Spectra Physics, Inc.) producing 1 mJ, 100 fs pulses at 800 nm. Frequency doubling a portion of the fundamental output in a BBO crystal produces 400 nm radiation at 120 μJ/pulse. The linearly polarized laser beam is mildly focused using a 2 m focal length lens positioned 1.3 m before the laser and ion beam crossing.

Photoelectron detection takes place in the direction perpendicular to both the ion and laser beams. A 40 mm diameter MCP detector with a P47 phosphor screen (Burle, Inc.) is mounted at the end of an internally μ-metal shielded electron flight tube. Images are obtained from the phosphor screen using a CCD camera (Roper Scientific, Inc.) and are typically averaged for (1–3) × 10⁴ experimental cycles. To discriminate against noise and backgrounds, the potential difference across the two imaging MCPs, normally maintained at 1.0–1.2 kV, is pulsed up to 1.8 kV for a 200 ns window timed to coincide with the arrival of the photoelectrons.

3. Results and Analysis

An overview of the 400 nm [(CO₂)_n(H₂O)_m][−] photoelectron images is presented in the form of an $n \times m$ table in Figure 1. The images corresponding to $m = 0$, $n = 4–9$ and $m = 1$, $n = 2–7$ have been presented previously.⁵⁹ They are included again here for completeness of the overall [(CO₂)_n(H₂O)_m][−] dataset. The contrast and/or brightness of some of the $m = 0$, $n = 4–9$ and $m = 1$, $n = 2–7$ images has been altered from the previous publication to highlight various important features but these images represent the same raw data as published previously. The laser polarization direction is vertical in the plane of all images. The effects of homogeneous and heterogeneous solvation can be examined through the (CO₂)_n[−] and [(CO₂)_n(H₂O)_m][−] image series of the top row and first column, respectively.

Most images display a single broad and anisotropic band corresponding to direct photodetachment. A few images, particularly those for CO₂[−]·H₂O, (CO₂)₂[−]·H₂O, and (CO₂)₂[−]·(H₂O)₂, also contain central spots corresponding to near-zero eKE electrons. In contrast to the thermionic emission⁶⁶ from covalently bound dimer-anion cores of (OCS)_n[−] and (CS₂)₂[−] cluster anions, the central features observed in the images presented here are laser independent. They therefore originate from autodetachment or field-induced detachment within the electron imaging lens. These signals were subtracted from the images and disregarded in the analysis.

Interesting new results obtained in this study are revealed in the photoelectron angular distributions. By inspection, the PADs remain qualitatively similar across each of the first three rows in Figure 1. For example, this is clearly evident for $m = 0$, the (CO₂)_n[−] cluster anions. The nature of the PADs from these clusters was discussed previously.^{59,60} A different trend is seen with the addition of more than two water molecules. Thus, unlike those for $m = 0–2$, the images in the fourth row in Figure 1 ($m = 3$) show a gradual decrease in the anisotropy with increasing n . An even more marked decrease in the anisotropy with increasing cluster size is seen in the first column, containing the CO₂[−]·(H₂O)_m, $m = 1–6$ images.

All images in Figure 1 are displayed on the same velocity scale, allowing for direct comparison by inspection of the corresponding eKE distributions. The consistent scaling of the images was achieved by using the same electrostatic potentials

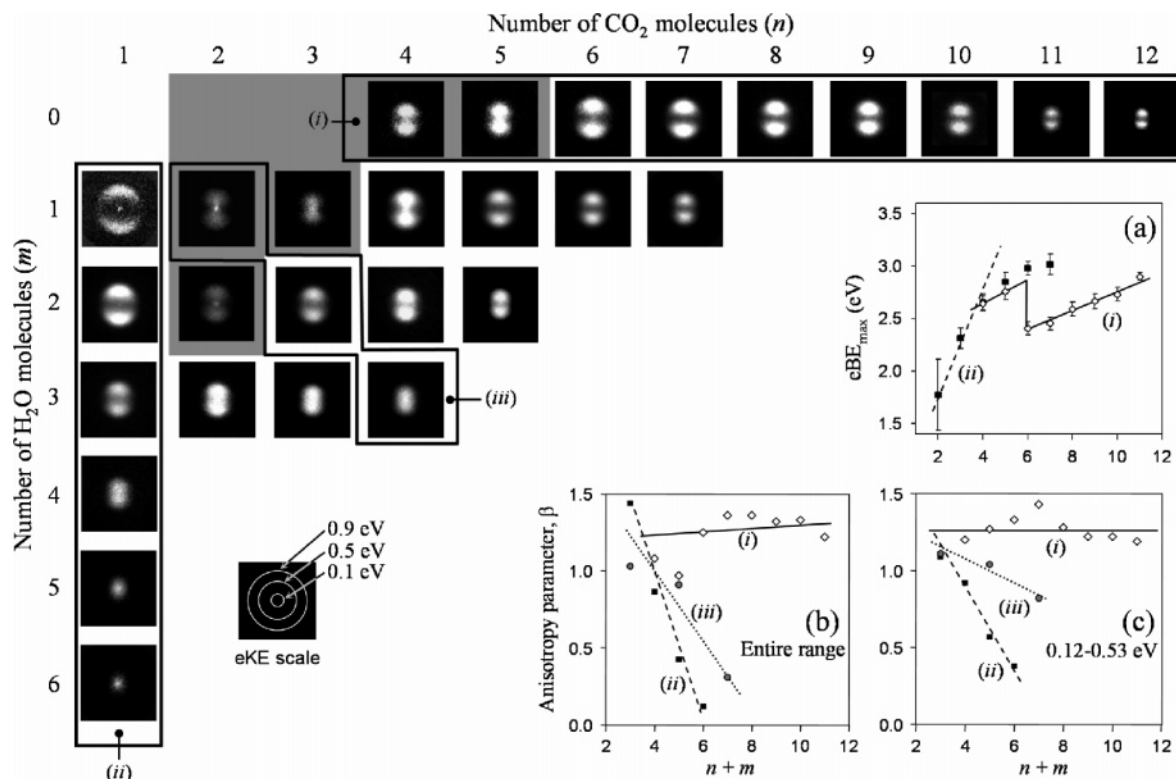


Figure 1. The 400 nm photoelectron images of $[(\text{CO}_2)_n(\text{H}_2\text{O})_m]^-$ cluster anions presented in the form of an $n \times m$ table. The images are shown on the same velocity scale, allowing for direct comparison of the corresponding photoelectron energies, according to the indicated eKE scale. The relative intensities of different images are arbitrary. The shaded part of the table marks the (n, m) domain corresponding to clusters with a predominance for covalent $(\text{CO}_2)_2^-$ cores (see the text for details). The solid frames around groups of images denote cluster series (i) $(\text{CO}_2)_n^-$, (ii) $[\text{CO}_2(\text{H}_2\text{O})_m]^-$, and (iii) $[(\text{CO}_2)_n(\text{H}_2\text{O})_{n-1}]^-$, as discussed in the text. Selected quantitative parameters obtained from the photoelectron images for the above cluster series are plotted in graphs (a)–(c) as functions of the total number of molecules in each cluster. The data for (i)–(iii) are shown as open diamonds, solid squares, and shaded circles, respectively. The solid, dashed and dotted lines through (i)–(iii) data, respectively, are drawn to guide the eye; they do not represent fits to the data. Graph (a) shows the $e\text{BE}_{\text{max}}$ values for (i) and (ii), with the error bars representing the standard deviations of the corresponding peak positions determined by fitting the experimental spectra with Gaussian profiles. Graphs (b) and (c) display the photoelectron anisotropy parameters β determined for (i)–(iii). In (b), the β parameter is determined by integrating over the entire energy range in the corresponding images, whereas in (c) only the 0.12–0.53 eV range is included, uniform for all images.

on the imaging lens for all cluster anions studied, with the exception of $(\text{CO}_2)_{10}^-$. The latter cluster was examined under different velocity-mapping conditions, but the corresponding photoelectron image was subsequently rescaled for consistency with the rest of the data.

The photoelectron bands generally shrink toward the image center as the size of the clusters increases. This trend is observed both across the rows and down the columns in the table of images in Figure 1. The shift toward smaller eKEs reflects the energetics of anion solvation. However, there are several notable exceptions from this general behavior, clearly seen in Figure 1 as a result of stepwise solvation by CO_2 , as well as stepwise hydration. For example, previous work⁵⁹ has shown that in the $(\text{CO}_2)_n^-$ series, the $n = 6$ detachment band covers a larger portion of the detector than that for $n = 5$, suggesting a lower detachment energy for the larger-size cluster. This discontinuity in vertical detachment energy (VDE), uncharacteristic of conventional solvation, has been seen as evidence of the dimer-to-monomer core switching in $(\text{CO}_2)_n^-$ occurring at $n = 6$.^{5,6,9,59} A similar discontinuity was observed in the $(\text{CO}_2)_n^- \cdot \text{H}_2\text{O}$ series between $n = 3$ and 4,⁵⁹ in agreement with the photoelectron spectroscopic study of Kondow and co-workers.⁹ Following past work,⁸ we refer to clusters with the CO_2^- and $(\text{CO}_2)_2^-$ cores as types I and II, respectively.

In the current work, core-switching is observed for the first time in the $[(\text{CO}_2)_n(\text{H}_2\text{O})_2]^-$ series (the third row of images in Figure 1) between $n = 2$ and 3. The discontinuity in relative image sizes in this series is a strong indication that the

$[(\text{CO}_2)_2(\text{H}_2\text{O})_2]^-$ cluster anions have predominantly type II cores, whereas those of $[(\text{CO}_2)_3(\text{H}_2\text{O})_2]^-$ are mainly type I. As discussed in more depth in the following section, this assertion also implies that the excess electron in the hydrated clusters with two H_2O molecules is localized on carbon dioxide.

Examining the stepwise-hydration series represented by columns in the table of images in Figure 1, we also note several discontinuities in image size, for example, between $(\text{CO}_2)_3^- \cdot \text{H}_2\text{O}$ and $(\text{CO}_2)_3^- \cdot (\text{H}_2\text{O})_2$ and between $(\text{CO}_2)_{4,5}^-$ and $(\text{CO}_2)_{4,5}^- \cdot \text{H}_2\text{O}$. Combining these observations with the known type II structures of $(\text{CO}_2)_2^-$ and $(\text{CO}_2)_3^-$ ^{5,12} allows us to define the domain within the (n, m) number space that corresponds to $[(\text{CO}_2)_n(\text{H}_2\text{O})_m]^-$ cluster anions with covalently bound $(\text{CO}_2)_2^-$ cluster cores. The corresponding area is indicated by a gray background in the table of images in Figure 1. Core-switching occurs when the boundaries of the shaded area are crossed.

The boundaries of the “type II” domain in the (n, m) number space are somewhat ambiguous, because of the coexistence of different core types observed for some of the cluster anions, and matters are further complicated by the dependence of the relative isomer abundances on the conditions of the ion source. For example, both types I and II structures are known to coexist for $(\text{CO}_2)_6^-$.^{5,7} The $(\text{CO}_2)_6^-$ photoelectron image in Figure 1 is noticeably larger than that for $(\text{CO}_2)_5^-$ because of the contribution of the monomer-based (type I) clusters with lower VDE (compared to the corresponding type II VDE). This does not, however, exclude a contribution of the dimer-based (type II) $(\text{CO}_2)_6^-$ clusters, as the corresponding photoelectron band lies

closer to the image center, partially concealed underneath the stronger monomer-based signal. A close examination of the (CO₂)₆⁻ image does in fact reveal a contribution of a low-eKE component, indicating a contribution of the dimer-based clusters to this particular image. However, because the monomer-based signal dominates in the image, the (6, 0) cell of the (*n*, *m*) number space is shown as belonging to the type I domain.

Similarly, coexistence of type I and type II structures was observed for several of the hydrated species,⁸ including, for example, (CO₂)₄⁻·H₂O. The corresponding image in Figure 1 lies outside of the type II domain, although the analysis does reveal a small contribution of the type II component to the photoelectron spectrum, in agreement with the work of Tsukuda et al.⁸

In summary, the shaded “type II” area in Figure 1 is drawn as a general guide to the dominant contributions of the dimer-based clusters, based on qualitative trends in the relative sizes of the adjacent photoelectron images. The boundaries of this domain, as drawn in the figure, do not take into account the coexistence of isomers for many of the species studied. Finally, we note that a reverse core switching from the monomer- to dimer-based clusters was observed in the (CO₂)_{*n*}⁻ series when the cluster size exceeds *n* = 13,⁷ but this size range is beyond the scope of the data set presented in Figure 1.

The photoelectron spectra and angular distributions were analyzed quantitatively through the inverse Abel transformation of the images,⁵⁷ using Reisler and co-workers’ Basis Set Expansion method.⁶⁷ The bands in the energy-domain spectra were fitted with Gaussian functions, allowing for systematic characterization of the cluster energetics. Graph (a) in Figure 1 presents selected values of electron binding energy (eBE = *hν* - eKE) corresponding to the peaks of the fitted spectral profiles (eBE_{max}). The eBE_{max} values are plotted versus the total number of molecular moieties in the cluster, *n* + *m*, for two cluster series: (i) (CO₂)_{*n*}⁻, *n* = 4–11 and (ii) CO₂⁻·(H₂O)_{*m*}, *m* = 2–6. The error bars reflect the standard deviations determined from the fits.

The maxima of photodetachment bands are commonly ascribed to the energy of the corresponding vertical detachment transitions. However, due to the varying contributions of the electronic cross-sections and Franck–Condon factors, the eBE_{max} do not necessarily reflect the corresponding VDEs. For example, if the VDE exceeds the photon energy used in the experiment, as in many cases here, the observed spectral maximum lies necessarily below the vertical transition energy, yielding an eBE_{max} that is smaller than the VDE. Hence, the values of eBE_{max} are lower bounds of the VDEs. Although both parameters reflect the same general energetic trends, the eBE_{max} values are additionally limited by the detachment photon energy. It is due to this upper limit that the eBE_{max} dependence for [CO₂(H₂O)_{*m*}]⁻, shown in Figure 1a, levels off for large clusters at an asymptote corresponding to the 3.1 eV photon energy.

In our previous work,^{47,59,68} we used an approximate *s*-wave correction for the detachment cross-section (eKE^{1/2}) based on the Wigner law⁶⁹ to extrapolate the VDE, but for low signal-to-noise spectra this procedure may be unreliable. Given the variation in the signal-to-noise ratio across the [(CO₂)_{*n*}(H₂O)_{*m*}]⁻ cluster series and for internal consistency within the whole dataset presented in this work, we have chosen to report the values of eBE_{max} [Figure 1a] rather than the VDEs. The former are derived from the data without reliance on a threshold scaling model and extrapolation; therefore, they allow for a more straightforward comparison of the energetic trends than VDEs. Because the eBE_{max} values in general do not correspond exactly

to the VDEs, the values reported here differ from the VDEs for some of the same cluster anions given in ref 59, even though both energetic parameters are obtained from the same raw data.

The angular distributions are characterized in terms of the anisotropy parameter β describing one-photon detachment with linearly polarized light.^{70–73} The PADs and thus β are generally eKE dependent. (b) and (c) in Figure 1 display the β values determined for selected cluster anions versus *m* + *n*, the total number of molecular moieties in the cluster. In (b), the PADs were integrated over a broad energy range representative of the corresponding image, covering about 80% of its spectral profile. Reading the electronic-structural information from these data is complicated by the eKE dependence of β , as different data points in Figure 1b correspond to the distributions integrated over different energy ranges. In an attempt to account for the eKE effects, the PADs were also analyzed within the limited eKE range from 0.12 to 0.53 eV, consistent for all clusters studied. This range is chosen because it contains significant signals in most of the reported images. The corresponding β values are plotted in graph (c) in Figure 1. Because the energy range is consistent throughout the data, Figure 1c may give a more reliable, eKE-independent insight into the changes in the electronic structure of the cluster anions with increasing solvation. Nonetheless, the qualitative trends in the anisotropy parameter are similar in Figure 1b,c.

The data in graphs (b) and (c) correspond to three cluster anion series, labeled (i)–(iii) and indicated by solid frames around the corresponding groups of images in Figure 1. (i) and (ii) are the same as in graph (a), namely, (i) the homogeneously solvated cluster anions (CO₂)_{*n*}⁻, corresponding to the first row of images in Figure 1, and (ii) the hydrated carbon dioxide anions CO₂⁻·(H₂O)_{*m*}, corresponding to the first column in Figure 1. (iii) is the mixed [(CO₂)_{*n*}(H₂O)_{*n-1*}]⁻ cluster anions, corresponding to the main diagonal in the table of images in Figure 1. Some cluster ions falling into series (i) and (ii), namely, (CO₂)₁₂⁻, CO₂⁻·H₂O, and CO₂⁻·(H₂O)₆, are not included in the graphs, because the corresponding photoelectron spectra do not fall in the range of eKE = 0.12–0.53 eV corresponding to Figure 1c.

The analysis of the photodetachment anisotropy reinforces the qualitative observations made at the beginning of this section. In (b) and (c) in Figure 1, the β values for (i), the homogeneous (CO₂)_{*n*}⁻ cluster anions, remain substantially positive, without much systematic change as a function of the cluster size. To the contrary, in (ii), the CO₂⁻·(H₂O)_{*m*} cluster anions, stepwise hydration monotonically lowers the degree of photoelectron anisotropy. (iii) is an intermediate case, where the anisotropy of photodetachment diminishes with increasing cluster size, but not as rapidly as in (ii). Thus, it appears that the addition of CO₂ molecules in the presence of no more than two water molecules does not significantly affect the photodetachment anisotropy, whereas increasing hydration, particularly in excess of two water molecules, has a pronounced effect in rendering the PAD progressively more isotropic.

4. Discussion

The main experimental findings can be summarized as follows. The spatial extent of the detachment bands in the [(CO₂)_{*n*}(H₂O)_{*m*}]⁻ photoelectron images decreases with increasing cluster size, except when the cluster core “switches” from a dimer to a monomer anion. The anisotropy of the PADs remains qualitatively unchanged upon solvation by CO₂, unaffected (remarkably so^{59,60}) even by the core switching. In contrast, a steady decline of anisotropy with increasing hydration is observed in mixed CO₂–water cluster anions.

With the energetic effects largely accounted for, the changes in β in Figure 1c are attributed primarily to the effect of solvation/hydration on the molecular orbital from which the photoelectrons originate. The $(\text{CO}_2)_n^-$, $n = 7-12$ cluster anions are known to have monomer-anion cores.^{5,7} The similarity of the anisotropy properties of these and $[\text{CO}_2(\text{H}_2\text{O})_m]^-$, $m = 1-2$, images suggests that the latter clusters also have CO_2^- cores.^{9,59} In fact, the energetics of the photodetachment bands support CO_2^- -based structures for all $[\text{CO}_2(\text{H}_2\text{O})_m]^-$ cluster anions studied, as the $e\text{BE}_{\text{max}}$ values for $[\text{CO}_2(\text{H}_2\text{O})_m]^-$, $m = 1-6$, plotted in Figure 1a, are consistent with the stepwise hydration of CO_2^- .

However, the similarity in the anisotropy between $(\text{CO}_2)_n^-$ and $[\text{CO}_2(\text{H}_2\text{O})_m]^-$ diminishes rapidly with increasing cluster size. The PAD becomes nearly isotropic for clusters containing as few as 5–6 water molecules. This observation, contrasted with the pure $(\text{CO}_2)_n^-$ cluster anions, prompts a hypothesis that perhaps the excess electron density in the larger hydrated clusters shifts from the CO_2 to the water segment of the cluster.

This hypothesis is consistent with the markedly negative adiabatic electron affinity of CO_2 ^{49,50} and the demonstrated ability of pure water clusters to bind an excess electron. However, the ground state of the hydrated electron in bulk water is of s character⁷⁴ and the direct photodetachment should produce a predominantly p-wave photoelectron.³⁹ Although the cluster size range in this work is far from “bulk”, the PADs of the $[\text{CO}_2(\text{H}_2\text{O})_m]^-$ cluster anions do not show the trend toward an anisotropic p-wave distribution expected for electrons originating from an s-like hydrated-electron state.³⁷

Further weakness of the above hypothesis is revealed by comparing the present results to the photoelectron spectra of the hydrated-electron cluster anions, $(\text{H}_2\text{O})_m^-$. In particular, if we insist on assuming that the excess electron in $[(\text{CO}_2)_n(\text{H}_2\text{O})_m]^-$ is bound to the water network, the VDEs of $\text{CO}_2 \cdot (\text{H}_2\text{O})_m^-$ can be predicted by combining the known VDEs of $(\text{H}_2\text{O})_m^-$ with the solvent binding energy of a neutral CO_2 to a negatively charged cluster. From past work,^{38,42,50,75} the VDEs of all observed isomers of $(\text{H}_2\text{O})_m^-$ in the size range relevant here ($2 \leq m \leq 6$) are under 0.5 eV. In fact, even for larger clusters, up to $m = 15$, the VDEs are under 1 eV. Adding a neutral CO_2 molecule to a negatively charged cluster typically stabilizes the cluster by about 0.2 eV,⁷⁶ and so the predicted VDEs of $\text{CO}_2 \cdot (\text{H}_2\text{O})_m^-$, $m \leq 6$, would remain well under 1 eV. This is clearly inconsistent with the experimental $e\text{BE}_{\text{max}}$ in Figure 1a (series ii), which represent the lower bounds of the VDEs. Further evidence against the shifting of electron localization to the water network can be found in the fact that an electron spin resonance signature of CO_2^- has been reported in aqueous solution.⁷⁷

To obtain insight into the structures of $[\text{CO}_2(\text{H}_2\text{O})_m]^-$ clusters, quantum-chemical calculations were carried out using Gaussian 98.⁷⁸ The $m = 2-6$ geometries were optimized at the MP2 level of theory using the 6-31+G* basis set, starting from several initial trial geometries; the $m = 2$ geometry was further optimized using the 6-31++G** basis set. The calculations yielded several energetically close structural isomers for each cluster size. The resulting global-minimum structures are shown schematically in Figure 2. Notably, the excess electron in all cluster structures is localized on CO_2 . This is true not only for the global-minimum geometries, but also for other low-energy isomers.

Considering the structures in Figure 2, the $\text{CO}_2^- (\text{H}_2\text{O})_2$ structure is qualitatively similar to that of the previously reported $\text{O}_3^- (\text{H}_2\text{O})_2$ anion,⁷⁹ whereas the $m = 3$ and 4 structures follow

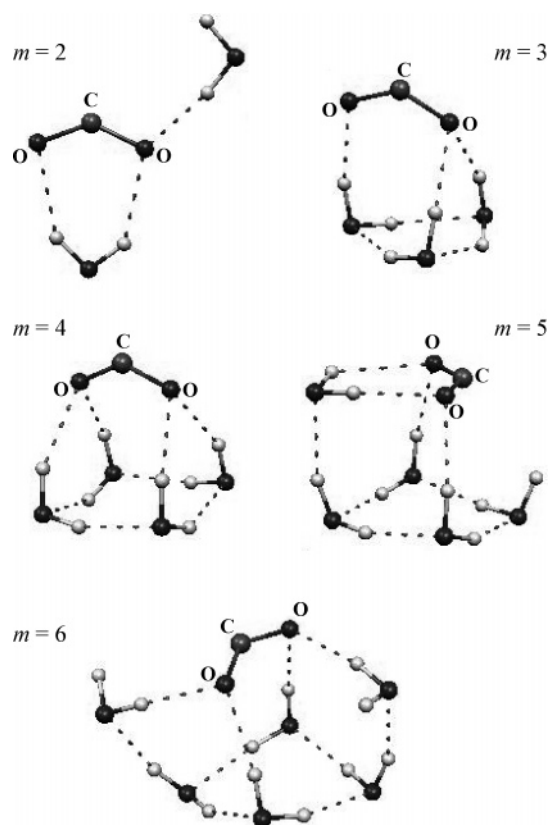


Figure 2. Sketches of the minimum-energy structures of $\text{CO}_2^- (\text{H}_2\text{O})_m$, $m = 2-6$ cluster anions, calculated as described in the text.

the same trend as the structures of hydrated iodide.^{21,80} In stepwise hydration of CO_2^- , the present calculations predict that the first water molecule forms two hydrogen bonds to the bent CO_2^- , forming a C_{2v} symmetry structure similar to that previously reported for $\text{CO}_2^- \cdot \text{H}_2\text{O}$.⁵² The second water forms just one hydrogen bond to the CO_2^- , giving a planar $\text{CO}_2^- (\text{H}_2\text{O})_2$ structure shown in Figure 2. In larger $\text{CO}_2^- (\text{H}_2\text{O})_m$ cluster anions, the third H_2O expands the water network into a ring of three water molecules, with all the dangling hydrogens binding to the CO_2^- solute. The fourth water molecule yields a ring of four essentially neutral H_2O molecules, with four hydrogen bonds to the solute, two for each oxygen of the CO_2^- . The fifth water departs from the ring-structure motif and binds directly to the CO_2^- , while also accepting a hydrogen bond from the $(\text{H}_2\text{O})_4$ ring. Two of the ring's other dangling hydrogens bind to the solute, and the fourth floats free. This configuration may be favored due to the high ring strain. The sixth water molecule binds to the solute and the water network.

Table 1 summarizes selected energetic parameters characterizing the global-minimum $[\text{CO}_2(\text{H}_2\text{O})_m]^-$, $m = 2-6$, structures, including the vertical detachment energies determined for the final geometries shown in Figure 2 by means of single-point MP2 calculations with the 6-311++G** basis set. The table compares the calculated VDEs with the experimentally determined peaks of the corresponding 400 nm detachment bands. As discussed above, these $e\text{BE}_{\text{max}}$ values represent lower bounds of the VDEs. Overall, the calculations underestimate the detachment energy of smaller, $m = 2-4$, clusters. For larger clusters ($m \geq 5$), the experimental $e\text{BE}_{\text{max}}$ values fall below the calculated VDE, because the VDEs for these clusters exceed the photon energy used in the experiment. The analysis of the orbitals calculated for $[\text{CO}_2(\text{H}_2\text{O})_m]^-$, $m = 2-6$, suggest that in all low-energy structures the excess electron remains localized on the CO_2 . This is evident from the Mulliken charges on CO_2 ,

TABLE 1: Energetics of the Global-Minimum Structures of the [CO₂(H₂O)_m]⁻ Cluster Anions from the MP2/6-311++G Calculations and Experimental Photoelectron Images alongside the Calculated Mulliken Charges on the Core CO₂ Moiety**

cluster anion	total energy (hartrees)	calc VDE (eV)	exp eBE _{max} (eV)	Mulliken charge on CO ₂
[CO ₂ (H ₂ O) ₂] ⁻	-340.76619	2.28	2.31 ± 0.10	-0.981
[CO ₂ (H ₂ O) ₃] ⁻	-417.06398	2.49	2.66 ± 0.08	-1.003
[CO ₂ (H ₂ O) ₄] ⁻	-493.36172	2.78	2.85 ± 0.09	-1.012
[CO ₂ (H ₂ O) ₅] ⁻	-569.65753	3.10	2.98 ± 0.07	-0.996
[CO ₂ (H ₂ O) ₆] ⁻	-645.95219	3.50	3.02 ± 0.10	-0.996

included in Table 1, determined for the [CO₂(H₂O)_m]⁻, $m = 2-6$, global minimum structures.

Thus, the calculations also do not support the hypothesis that the excess electron in the mixed [(CO₂)_n(H₂O)_m]⁻ clusters is bound to the water network. Hence, we find no evidence that any of the [CO₂(H₂O)_m]⁻ cluster anions studied here can be described as CO₂·(H₂O)_m⁻ and conclude that the experimental observations are consistent with the theoretically predicted CO₂⁻(H₂O)_m structures shown in Figure 2. In this view, it is most plausible that the structures of all [(CO₂)_n(H₂O)_m]⁻ cluster anions studied here are characterized by the excess electron localized on the carbon-dioxide part of the cluster, with the water molecules playing the role of a solvent. In this case, the molecular orbitals from which the observed photoelectrons originate have qualitatively the same structures as in pure (CO₂)_n⁻ cluster ions, i.e., either the monomer CO₂⁻ or the dimer (CO₂)₂⁻ orbitals.

Consequently, the diminishing photodetachment anisotropy observed for the (CO₂)_n⁻·(H₂O)_m cluster anions reflects the dynamics of electron detachment in the presence of water molecules, rather than the structure of the parent molecular orbitals. Straightforward mechanisms involve the effect of long-range interactions and/or an indirect detachment process. In the former scenario, the dipole moment of the neutral residue interacts strongly with the detached electron, affecting the partial detachment cross-sections^{69,81,82} and therefore the PAD.⁸³ However, it is unlikely that in this case the anisotropy would show a monotonic decrease to zero with increasing cluster size. In our recent discussion of the dipolar interactions in the photodetachment of solvated iodide, we also concluded that excited states rather than long-range interactions had the predominant effect on the photodetachment anisotropy.⁸⁴

This leaves indirect photodetachment as a likely explanation for the behavior of the (CO₂)_n⁻·(H₂O)_m PADs in this study. Under this mechanism, the excess electron in photoexcited hydrated clusters is first transferred to the water network, according to (CO₂)_n⁻·(H₂O)_m + $h\nu \rightarrow$ [(CO₂)_n·(H₂O)_m]^{-*}, which is followed by dissociative autodetachment of the excited cluster denoted by an asterisk. The delayed autodetachment is expected to yield an isotropic photoelectron angular distribution.

Similar processes have been observed in other cluster anions, such as solvated (as well as hydrated) iodide anions.^{4,30-34} Of particular relevance are the charge transfer to solvent (CTTS) transitions in I⁻(H₂O)_n, $n \geq 5$.⁴ The wavelength of light in the present experiments is in the right range for such transitions to occur. In fact, energetically, the photoinduced CTTS transitions of a (CO₂)_n⁻·(H₂O)_m \rightarrow [(CO₂)_n·(H₂O)_m]^{-*} kind should be even more feasible than in the case of hydrated I⁻, because of the lower VDEs of both CO₂⁻ and (CO₂)₂⁻ cluster cores. The (CO₂)_n⁻·(H₂O)_m⁻ electronic states are indeed available, as they represent the known (H₂O)_m⁻ hydrated-electron clusters, additionally solvated by CO₂. The CTTS transitions in (CO₂)_n⁻·(H₂O)_m would be cluster analogues of CTTS in liquids^{27,85} and their importance is expected to increase with increasing size of the water network. The observed trend of diminishing anisotropy

with increasing number of water molecules in the (CO₂)_n⁻·(H₂O)_m clusters is in line with this expectation.

5. Summary

Photoelectron images of hydrated carbon dioxide cluster anions demonstrate the effects of homogeneous and heterogeneous solvation on the electronic structure and photodetachment dynamics. The homogeneous solvation in pure (CO₂)_n⁻ cluster anions with n up to 12 has minimal effect on the photoelectron angular distributions, even when the core switching occurs at $n = 6$. The heterogeneous hydration, on the other hand, has a marked effect of erasing the photodetachment anisotropy. The analysis of the data, supported by theoretical modeling, indicates that in the initial, ground electronic state of these hydrated cluster anions the excess electron is localized on carbon dioxide. The diminishing photoelectron anisotropy is proposed to be attributable to the charge-transfer-to-solvent transitions, creating a transient (CO₂)_n⁻·(H₂O)_m⁻ state that subsequently decays via autodetachment. Photodetachment using higher-energy photons might be expected to delay the onset of diminishing anisotropy, because the ejected electrons would be produced with greater kinetic energy. Thus, future measurements at a shorter photon wavelength will provide a valuable test of the CTTS hypothesis.

Acknowledgment. We gratefully acknowledge the support by the National Science Foundation (grant No. CHE-0134631), the Arnold and Mabel Beckman Foundation (Beckman Young Investigator Award), the David and Lucile Packard Foundation (Packard Fellowship for Science and Engineering), and the Camille and Henry Dreyfus Foundation (Camille Dreyfus Teacher-Scholar Award).

References and Notes

- (1) Castleman, A. W.; Wei, S. *Annu. Rev. Phys. Chem.* **1994**, *45*, 685.
- (2) Castleman, A. W.; Bowen, K. H. *J. Phys. Chem.* **1996**, *100*, 12911.
- (3) Sanov, A.; Lineberger, W. C. *PhysChemComm* **2002**, 165.
- (4) Lehr, L.; Zanni, M. T.; Frischkorn, C.; Weinkauff, R.; Neumark, D. M. *Science* **1999**, *284*, 635.
- (5) DeLuca, M. J.; Niu, B.; Johnson, M. A. *J. Chem. Phys.* **1988**, *88*, 5857.
- (6) Nagata, T.; Yoshida, H.; Kondow, T. *Chem. Phys. Lett.* **1992**, *199*, 205.
- (7) Tsukuda, T.; Johnson, M. A.; Nagata, T. *Chem. Phys. Lett.* **1997**, *268*, 429.
- (8) Tsukuda, T.; Saeki, M.; Kimura, R.; Nagata, T. *J. Chem. Phys.* **1999**, *110*, 7846.
- (9) Nagata, T.; Yoshida, H.; Kondow, T. *Z. Phys. D* **1993**, *26*, 367.
- (10) Tsukuda, T.; Hirose, T.; Nagata, T. *Chem. Phys. Lett.* **1997**, *279*, 179.
- (11) Sanov, A.; Nandi, S.; Jordan, K. D.; Lineberger, W. C. *J. Chem. Phys.* **1998**, *109*, 1264.
- (12) Fleischman, S. H.; Jordan, K. D. *J. Phys. Chem.* **1987**, *91*, 1300.
- (13) Sanov, A.; Lineberger, W. C.; Jordan, K. D. *J. Phys. Chem. A* **1998**, *102*, 2509.
- (14) Arnold, D. W.; Bradforth, S. E.; Kim, E. H.; Neumark, D. M. *J. Chem. Phys.* **1992**, *97*, 9468.
- (15) Zhao, Y. X.; Arnold, C. C.; Neumark, D. M. *J. Chem. Soc., Faraday Trans.* **1993**, *89*, 1449.
- (16) Arnold, D. W.; Bradforth, S. E.; Kim, E. H.; Neumark, D. M. *J. Chem. Phys.* **1995**, *102*, 3493.

- (17) Osterwalder, A.; Nee, M. J.; Zhou, J.; Neumark, D. M. *J. Chem. Phys.* **2004**, *121*, 6317.
- (18) Weber, J. M.; Schneider, H. *J. Chem. Phys.* **2004**, *120*, 10056.
- (19) Bailey, C. G.; Kim, J.; Dessent, C. E. H.; Johnson, M. A. *Chem. Phys. Lett.* **1997**, *269*, 122.
- (20) Ayotte, P.; Weddle, G. H.; Kim, J.; Johnson, M. A. *Chem. Phys.* **1998**, *239*, 485.
- (21) Ayotte, P.; Weddle, G. H.; Kim, J.; Kelley, J.; Johnson, M. A. *J. Phys. Chem. A* **1999**, *103*, 443.
- (22) Ayotte, P.; Weddle, G. H.; Johnson, M. A. *J. Chem. Phys.* **1999**, *110*, 7129.
- (23) Ayotte, P.; Nielsen, S. B.; Weddle, G. H.; Johnson, M. A.; Xantheas, S. S. *J. Phys. Chem. A* **1999**, *103*, 10665.
- (24) Corcelli, S. A.; Kelley, J. A.; Tully, J. C.; Johnson, M. A. *J. Phys. Chem. A* **2002**, *106*, 4872.
- (25) Woronowicz, E. A.; Robertson, W. H.; Weddle, G. H.; Johnson, M. A.; Myshakin, E. M.; Jordan, K. D. *J. Phys. Chem. A* **2002**, *106*, 7086.
- (26) Jortner, J.; Ottolenghi, M.; Stein, G. *J. Phys. Chem.* **1964**, *68*, 247.
- (27) Bradforth, S. E.; Jungwirth, P. *J. Phys. Chem. A* **2002**, *106*, 1286.
- (28) Becker, I.; Markovich, G.; Cheshnovsky, O. *Phys. Rev. Lett.* **1997**, *79*, 3391.
- (29) Becker, I.; Cheshnovsky, O. *J. Chem. Phys.* **1999**, *110*, 6288.
- (30) Serxner, D.; Dessent, C. E. H.; Johnson, M. A. *J. Chem. Phys.* **1996**, *105*, 7231.
- (31) Zanni, M. T.; Frischkorn, C.; Davis, A. V.; Neumark, D. M. *J. Phys. Chem. A* **2000**, *104*, 2527.
- (32) Frischkorn, C.; Zanni, M. T.; Davis, A. V.; Neumark, D. M. *Faraday Discuss.* **2000**, *115*, 49.
- (33) Chen, H. Y.; Sheu, W. S. *J. Am. Chem. Soc.* **2000**, *122*, 7534.
- (34) Davis, A. V.; Zanni, M. T.; Frischkorn, C.; Neumark, D. M. *J. Electron Spectrosc. Relat. Phenom.* **2000**, *108*, 203.
- (35) Hart, E. J.; Boag, J. W. *J. Am. Chem. Soc.* **1962**, *84*, 4090.
- (36) Posey, L. A.; DeLuca, M. J.; Campagnola, P. J.; Johnson, M. A. *J. Phys. Chem.* **1989**, *93*, 1178.
- (37) Bragg, A. E.; Verlet, J. R. R.; Kammrath, A.; Cheshnovsky, O.; Neumark, D. M. *Science* **2004**, *306*, 669.
- (38) Kim, J.; Becker, I.; Cheshnovsky, O.; Johnson, M. A. *Chem. Phys. Lett.* **1998**, *297*, 90.
- (39) Campagnola, P. J.; Posey, L. A.; Johnson, M. A. *J. Chem. Phys.* **1990**, *92*, 3243.
- (40) Bailey, C. G.; Kim, J.; Johnson, M. A. *J. Phys. Chem.* **1996**, *100*, 16782.
- (41) Ayotte, P.; Weddle, G. H.; Bailey, C. G.; Johnson, M. A.; Vila, F.; Jordan, K. D. *J. Chem. Phys.* **1999**, *110*, 6268.
- (42) Lee, G. H.; Arnold, S. T.; Eaton, J. G.; Sarkas, H. W.; Bowen, K. H.; Ludewigt, C.; Haberland, H. *Z. Phys. D* **1991**, *20*, 9.
- (43) Saeki, M.; T., T.; Nagata, T. *Chem. Phys. Lett.* **2001**, *348*, 461.
- (44) Saeki, M.; Tsukuda, T.; Nagata, T. *Chem. Phys. Lett.* **2001**, *340*, 376.
- (45) Negishi, Y.; Nagata, T.; Tsukuda, T. *Chem. Phys. Lett.* **2002**, *364*, 127.
- (46) Surber, E.; Ananthavel, S. P.; Sanov, A. *J. Chem. Phys.* **2002**, *116*, 1920.
- (47) Surber, E.; Sanov, A. *J. Chem. Phys.* **2002**, *116*, 5921.
- (48) Gutsev, G. L.; Bartlett, R. J.; Compton, R. N. *J. Chem. Phys.* **1998**, *108*, 6756.
- (49) Compton, R. N.; Reinhardt, P. W.; Cooper, C. D. *J. Chem. Phys.* **1975**, *63*, 3821.
- (50) Bowen, K. H.; Eaton, J. G. Photodetachment Spectroscopy of Negative Cluster Ions. In *The Structure of Small Molecules and Ions*; Naaman, R., Vager, Z., Eds.; Plenum: New York, 1988; p 147.
- (51) Klots, C. E. *J. Chem. Phys.* **1979**, *71*, 4172.
- (52) Saeki, M.; Tsukuda, T.; Iwata, S.; Nagata, T. *J. Chem. Phys.* **1999**, *111*, 6333.
- (53) Pinare, J. C.; Baguenard, B.; Bordas, C.; Broyer, M. *Eur. Phys. J. D* **1999**, *9*, 21.
- (54) Surber, E.; Mabbs, R.; Sanov, A. *J. Phys. Chem. A* **2003**, *107*, 8215.
- (55) Mabbs, R.; Surber, E.; Sanov, A. *Analyst* **2003**, *128*, 765.
- (56) Chandler, D. W.; Houston, P. L. *J. Chem. Phys.* **1987**, *87*, 1445.
- (57) Heck, A. J. R.; Chandler, D. W. *Annu. Rev. Phys. Chem.* **1995**, *46*, 335.
- (58) Ervin, K. M.; Lineberger, W. C. Photoelectron Spectroscopy of Negative Ions. In *Advances in Gas-Phase Ion Chemistry*; Adams, N. G., Babcock, L. M., Eds.; JAI Press: Greenwich, U.K., 1992; Vol. 1, p 121.
- (59) Mabbs, R.; Surber, E.; Velarde, L.; Sanov, A. *J. Chem. Phys.* **2004**, *120*, 5148.
- (60) Mabbs, R.; Surber, E.; Sanov, A. *Chem. Phys. Lett.* **2003**, *381*, 479.
- (61) Johnson, M. A.; Lineberger, W. C. Pulsed Methods for Cluster Ion Spectroscopy. In *Techniques for the Study of Ion-Molecule Reactions*; Farrar, J. M., Saunders, W. H., Eds.; Wiley: New York, 1988; p 591.
- (62) Nadal, M. E.; Kleiber, P. D.; Lineberger, W. C. *J. Chem. Phys.* **1996**, *105*, 504.
- (63) Eppink, A. T. J. B.; Parker, D. H. *Rev. Sci. Instrum.* **1997**, *68*, 3477.
- (64) Wiley, W. C.; McLaren, I. H. *Rev. Sci. Instrum.* **1955**, *26*, 1150.
- (65) Posey, L. A.; DeLuca, M. J.; Johnson, M. A. *Chem. Phys. Lett.* **1986**, *131*, 170.
- (66) Andersen, J. U.; Bonderup, E.; Hansen, K. *J. Phys. B* **2002**, *35*, R1.
- (67) Dribinski, V.; Ossadtchi, A.; Mandelshtam, V. A.; Reisler, H. *Rev. Sci. Instrum.* **2002**, *73*, 2634.
- (68) Surber, E.; Sanov, A. *J. Chem. Phys.* **2003**, *118*, 9192.
- (69) Wigner, E. P. *Phys. Rev.* **1948**, *73*, 1002.
- (70) Cooper, J.; Zare, R. N. Photoelectron angular distributions. In *Atomic collision processes*; Geltman, S., Mahanthappa, K. T., Brittin, W. E., Eds.; Gordon and Breach, Science Publishers: New York, London, Paris, 1968; Vol. XI-C, p 317.
- (71) Cooper, J.; Zare, R. N. *J. Chem. Phys.* **1968**, *48*, 942.
- (72) Cooper, J.; Zare, R. N. *J. Chem. Phys.* **1968**, *49*, 4252.
- (73) Zare, R. N. *Mol. Photochem.* **1972**, *4*, 1.
- (74) Schnitker, J.; Motakabbir, K.; Rossky, P. J.; Friesner, R. *Phys. Rev. Lett.* **1988**, *60*, 456.
- (75) Coe, J. V.; Lee, G. H.; Eaton, J. G.; Arnold, S. T.; Sarkas, H. W.; Bowen, K. H.; Ludewigt, C.; Haberland, H.; Worsnop, D. R. *J. Chem. Phys.* **1990**, *92*, 3980.
- (76) Sanov, A.; Lineberger, W. C. *Phys. Chem. Chem. Phys.* **2004**, *6*, 2018.
- (77) Symons, M. C. R.; Zimmerman, D. N. *Int. J. Radiat. Phys. Chem.* **1976**, *8*, 595.
- (78) Frisch, M. J.; Trucks, G. W.; Schlegel, H. B.; Scuseria, G. E.; Robb, M. A.; Cheeseman, J. R.; Zakrzewski, V. G.; Montgomery, J. A., Jr.; Stratmann, R. E.; Burant, J. C.; Dapprich, S.; Millam, J. M.; Daniels, A. D.; Kudin, K. N.; Strain, M. C.; Farkas, O.; Tomasi, J.; Barone, V.; Cossi, M.; Cammi, R.; Mennucci, B.; Pomelli, C.; Adamo, C.; Clifford, S.; Ochterski, J.; Petersson, G. A.; Ayala, P. Y.; Cui, Q.; Morokuma, K.; Malick, D. K.; Rabuck, A. D.; Raghavachari, K.; Foresman, J. B.; Cioslowski, J.; Ortiz, J. V.; Stefanov, B. B.; Liu, G.; Liashenko, A.; Piskorz, P.; Komaromi, I.; Gomperts, R.; Martin, R. L.; Fox, D. J.; Keith, T.; Al-Laham, M. A.; Peng, C. Y.; Nanayakkara, A.; Gonzalez, C.; Challacombe, M.; Gill, P. M. W.; Johnson, B. G.; Chen, W.; Wong, M. W.; Andres, J. L.; Head-Gordon, M.; Replogle, E. S.; Pople, J. A. *Gaussian 98*, revision A.7; Gaussian, Inc.: Pittsburgh, PA, 1998.
- (79) Bentley, J.; Collins, J. Y.; Chipman, D. M. *J. Phys. Chem. A* **2000**, *104*, 4629.
- (80) Vila, F. D.; Jordan, K. D. *J. Phys. Chem. A* **2002**, *106*, 1391.
- (81) Mead, R. D.; Lykke, K. R.; Lineberger, W. C. Photodetachment Threshold Laws. In *Electronic and Atomic Collisions*; Eichler, J., Hertel, I. V., Stolterfoht, N., Eds.; Elsevier: 1984; p 721.
- (82) Farley, J. W. *Phys. Rev. A* **1989**, *40*, 6286.
- (83) O'Malley, T. F. *Phys. Rev.* **1965**, *137*, A1668.
- (84) Mabbs, R.; Surber, E.; Sanov, A. *J. Chem. Phys.* **2005**, *122*, 054308.
- (85) Crowell, R. A.; Lian, R.; Shkrob, I. A.; Bartels, D. M.; Chen, X. Y.; Bradforth, S. E. *J. Chem. Phys.* **2004**, *120*, 11712.